MSDE

COMMUNICATION

View Article Online
View Journal | View Issue

Cite this: *Mol. Syst. Des. Eng.*, 2025, 10, 7

Received 30th June 2024,
Accepted 11th November 2024

DOI: 10.1039/d4me00105b

rsc.li/molecular-engineering

Dual-labelled polymeric micelles for singlet oxygen reporting in biological systems†

Yasuhiro Nakagawa, ‡[abc] Hayato Laurence Mizuno,[bc] Yuta Ushimaru,[a] Jumpei Norimatsu,[a] Kazunori Igarashi,[ab] Keita Masuda,[a] Madoka Takai,[a] Yasutaka Anraku[bc] and Horacio Cabral *[ab]

Visualizing singlet oxygen ($^1O_2$) in biological systems could greatly enhance our understanding of its biological roles and offer new diagnostics and therapeutics. However, $^1O_2$ is unstable and highly reactive, making its detection in living systems a significant challenge. To address this, we have developed dually-labelled polymeric micelles designed to trace both the location and levels of $^1O_2$.

Reactive oxygen species (ROS), *e.g.*, super oxide anions (O_2^-), hydrogen peroxide (H_2O_2), and $^1O_2$, are important mediators in a variety of biological and pathological processes.[1,2] The ROS are involved in essential biological functions, such as signalling, metabolism, and regulation of the immune system.[3] When ROS are overproduced or antioxidants are depleted, these reactive species cause oxidative stress, oxidizing lipids, proteins, carbohydrates, RNA, and DNA, which leads to cellular damage. Such damage is linked to various diseases, including cardiovascular disease, neurodegenerative disorders, and cancer.[4–7] Moreover, high ROS levels can be used for therapeutically damaging cancer cells.[8] In fact, a major physiological mechanism to kill tumour cells is the production of ROS by neutrophils and macrophages.[9] Moreover, certain anticancer drugs can induce ROS production. For instance, oxaliplatin, a widely used chemotherapeutic agent,[10] can directly affect mitochondria, inducing mitochondrial permeability transition and ROS generation.[11,12] Thus, an improved understanding of the role of ROS in living systems can provide opportunities for developing innovative diagnostic and therapeutic strategies.

Design, System, Application

Singlet oxygen ($^1O_2$) plays a crucial role in various biological processes, including cellular signaling and oxidative stress, necessitating reliable methods for its detection and quantification. However, detecting $^1O_2$ in biological systems is challenging due to its high reactivity and short lifespan. Here, we developed dually-labelled polymeric micelles (SOSG@Cy5-PIC/m) capable of detecting $^1O_2$ and reporting probe positions. These micelles are formed using oppositely charged diblock copolymers, Cy5-conjugated PEG-poly(α,β-aspartic acid) and Cy5-conjugated PEG[1]poly([5-aminopentyl]-α,β-aspartamide), which self-assemble in aqueous solution. Singlet oxygen sensor green (SOSG) molecules, which fluoresce upon interaction with $^1O_2$, are integrated into the micelle core by condensation to the amines in the poly([5-aminopentyl]-α,β-aspartamide) block. The micelle core is crosslinked by forming amide bonds between the carboxylates in the poly(α,β[1] aspartic acid) segment and the amines in the poly([5-aminopentyl]-α,β-aspartamide) block, ensuring stability in biological environments. The micelles are around 30 nm and the dyes in their core are protected by a dense PEG shell. The micelles quantitatively detect $^1O_2$ in media and enable visualization of $^1O_2$ in 3D cellular spheroids under induced cellular stress. Potential applications include advancing research tools for understanding $^1O_2$, diagnostics for oxidative stress-related diseases and exploring targeted therapies, such as photodynamic therapy. Future developments may enhance sensitivity and targeting capabilities for broader biomedical applications.

Detection of $^1O_2$ has been attracting much attention, as it is involved in various biological phenomena by direct reaction with biomolecules and regulation of intracellular signals.[13,14] However, because $^1O_2$ has a short lifetime, high reactivity, and low concentration, its detection has been challenging. Several approaches have been developed for the detection of $^1O_2$, including direct measurement of $^1O_2$ phosphorescence (transition light from singlet to triplet state) at 1280 nm,[15] electron spin resonance spectroscopy (ESR),[16] photo/chromo-sensitizers,[17] and fluorescent probes.[18] Despite these major efforts, *in situ* observation is still limited. Challenges include low phosphorescence quantum efficiency (~10^{-6} for aqueous systems and even smaller for systems containing $^1O_2$ quencher),[19] inefficient conversion of $^1O_2$ to stable radical species for ESR,[16] toxicity and cellular damage

[a] *Department of Bioengineering, Graduated School of Engineering, The University of Tokyo, 7-3-1 Hongo, Bunkyo-ku, Tokyo, 113-8656, Japan.*
E-mail: horacio@bmw.t.u-tokyo.ac.jp
[b] *Innovation Center of NanoMedicine, Kawasaki Institute of Industrial Promotion, 3-25-14 Tonomachi, Kawasaki-ku, Kawasaki, 210-0821, Japan*
[c] *Department of Materials Science and Engineering, Graduated School of Materials and Chemical Technology, Tokyo Institute of Technology, 2-12-1 Ookayama, Meguro-ku, Tokyo, 152-8550, Japan*

† Electronic supplementary information (ESI) available: Materials and methods. See DOI: https://doi.org/10.1039/d4me00105b

‡ Y. N. has moved to Mitsui Chemicals, Inc. (Tokyo, Japan).

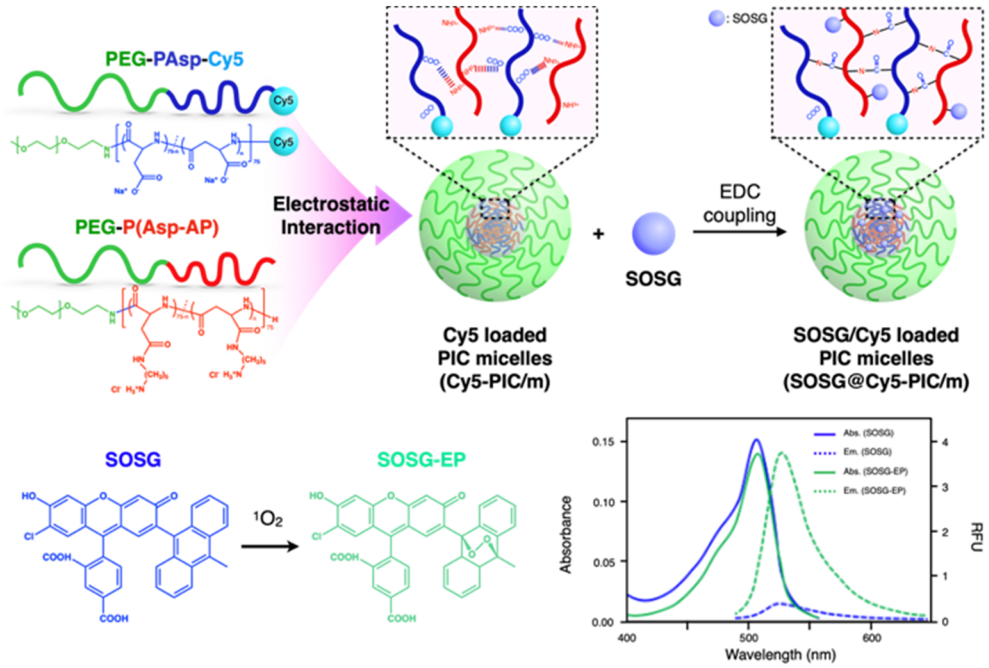

Fig. 1 Schematic illustration of SOSG/Cy5-labeled PIC micelles (SOSG@Cy5-PIC/m). The conjugated SOSG enables the detection of $^1O_2$ by changing its fluorescent characteristic, while the Cy5 constantly reports the position of the probes in biological systems.

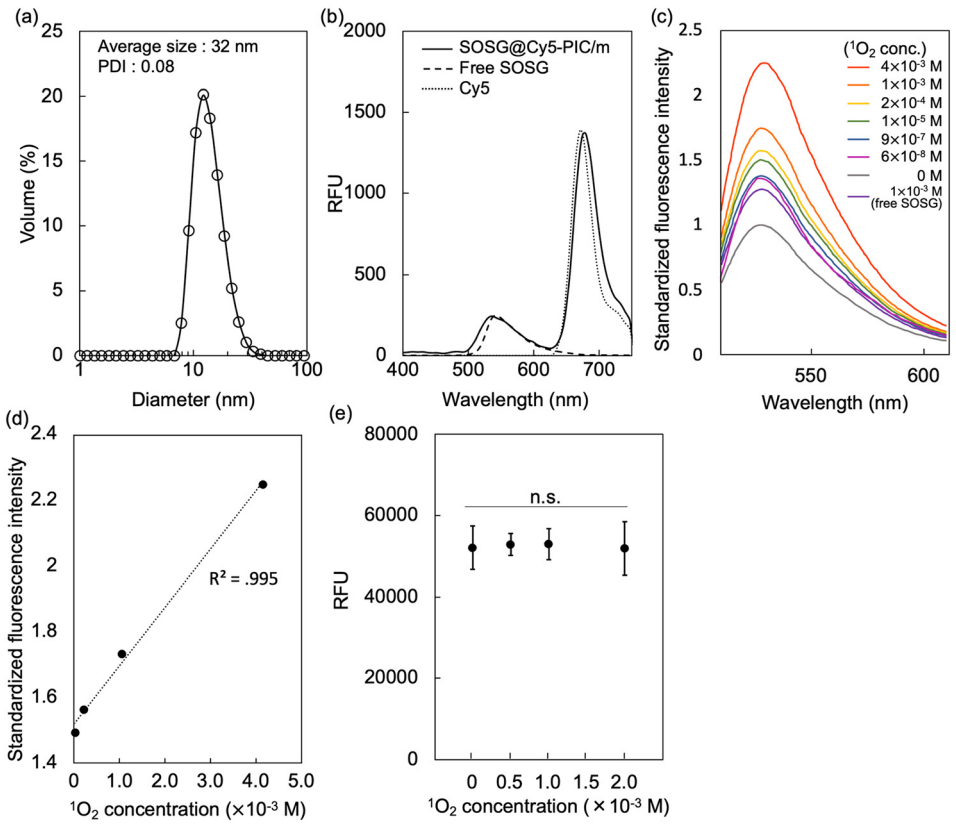

Fig. 2 Characterization of the SOSG@Cy5-labeled PIC/m (SOSG@Cy5-PIC/m). (a) Size distribution of SOSG@Cy5-PIC/m determined by DLS. (b) Fluorescent spectra of SOSG@Cy5-PIC/m, SOSG, and Cy5 (excitation (Ex) = 460 nm). (c) $^1O_2$ dose-dependent fluorescence intensity of SOSG@Cy5-PIC/m (Ex = 460 nm). (d) $^1O_2$ dose-dependent fluorescence intensity of SOSG@Cy5-PIC/m at an emission wavelength of 530 nm. (e) $^1O_2$ dose-dependent fluorescence intensity of Cy5 in PIC/m (Ex = 633 nm).

from photo/chromo-sensitizers,[20] and low stability and uncertain distribution of fluorescent probes in tissues and cells. Thus, innovative approaches are still necessary for effective $^1O_2$ sensing in biological systems.

Polymeric micelles, *i.e.*, core–shell polymeric structures, have demonstrated great potential for targeted therapy and diagnosis by delivering a wide variety of bioactive compounds loaded in their core.[21] Moreover, the shell of the polymeric micelles can protect the bioactive agents in the core from biological degradation. Thus, polymeric micelles can navigate and spatiotemporally control the function of the payloads in biological settings.[22] Polymeric micelles can be assembled in aqueous environments by controlling the interaction of the forming block copolymers, such as the hydrophobicity and electrostatic interaction between the core-forming segments. Particularly, polyion complex (PIC) micelles have been prepared using poly(ethylene glycol) (PEG) based oppositely-charged segments of the block copolymer pair of PEG-poly(anion) and PEG-poly(cation). These PIC micelles (PIC/m) offer substantial advantages as reporter agents, as they allow effective size control, softness, and versatile drug loading capability.[23]

Here, we developed a nano-scaled reporter based on PIC/m that is capable of indicating its distribution in living systems and sensing the presence of $^1O_2$ in their surroundings. These reporters were made by mixing oppositely charged diblock copolymers, *i.e.*, Cy5-conjugated PEG-poly(α,β-aspartic acid) (PEG-PAsp) and Cy5-conjugated PEG-poly([5-aminopentyl]-α,β-aspartamide) (PEG-P(Asp-AP)), in an aqueous solution.[24] The PIC/m were also stabilised by cross-linking the core through 1-ethyl-3-(3-dimethylaminopropyl)carbodiimide (EDC) coupling to avoid micelle dissociation in biological environments. As cross-linked PIC structures are still permeable to small biomolecules,[24] Singlet oxygen sensor green (SOSG) molecules, which are precise reporters of $^1O_2$,[25,26] were conjugated to the core of the micelles to provide specific sensitivity for fluorescent detection of $^1O_2$ (Fig. 1).[18] After purification to remove the unreacted SOSG and EDC, the size and polydispersity index of the dual-labelled micelles (SOSG@Cy5-PIC/m) were 31 nm and 0.08, respectively (Fig. 2a). The incorporation of Cy5 and SOSG was confirmed by fluorescence spectrometry (Fig. 2b), with the emission spectrum of the SOSG@Cy5-PIC/m showing peaks at 540 nm and 680 nm, corresponding to SOSG and Cy5, respectively. These results indicate successful preparation of SOSG@Cy5-PIC/m.

The $^1O_2$ detection capacity of SOSG@Cy5-PIC/m was evaluated by using endoperoxide (EP), which is a convenient reagent for this purpose, as it can quantitatively generate $^1O_2$ in solution by simply heating above 35 °C without using light or photosensitisers. The $^1O_2$ dose-dependent fluorescence emission

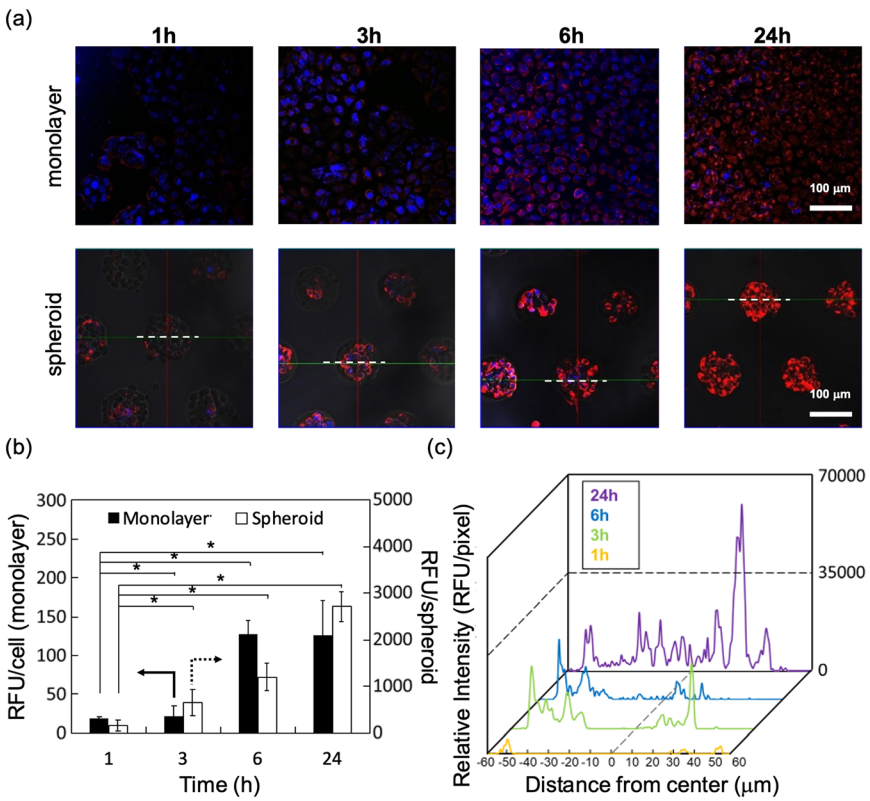

Fig. 3 (a) Time-lapse images of monolayer/spheroidal cultured BxPC3 cells with SOSG@Cy5-PIC/m observed by confocal laser-scanning microscopy (blue: nuclei [Ex/emission (Em) = 405/446 nm], red: SOSG@Cy5-PIC/m [Ex/Em = 633/661–750 nm]). (b) Time-dependent uptake of SOSG@Cy5-PIC/m for single cell/spheroid against monolayer/spheroidal cultured BxPC3 cells (n = 3), and all plots were statistically analysed by the Tukey–Kramer method (*$p < 0.005$). (c) Quantification of internalised SOSG@Cy5-PIC/m against BxPC-3 spheroid. The relative intensity (RFU per pixel) is calculated from the pixel-by-pixel integration of the RFU on the white dotted line in Fig. 3(a) (spheroid).

of SOSG@Cy5-PIC/m showed a gradual increase of the peak at 539 nm (Fig. 2c), similar to the behavior observed with free SOSG. The fluorescence intensity of SOSG@Cy5-PIC/m was stronger than that of free SOSG under 1×10^{-3} M $^1O_2$ presumably due to reduced inter-SOSG energy transfer that caused quenching of free SOSG. The increase in fluorescence intensity exhibited high linearity in relation to $^1O_2$ concentration, indicating that the micelles can quantitatively detect $^1O_2$ (Fig. 2d). Importantly, the Cy5 fluorescence remained unaffected by $^1O_2$ levels (Fig. 2e), reinforcing its reliability as a stable marker for PIC/m concentration. This stability enables the use of Cy5 fluorescence to normalize SOSG signal, providing a robust ratiometric approach for precise quantification of $^1O_2$ in biological samples.

The time-dependent cellular uptake of SOSG@Cy5-PIC/m was examined in monolayer and spheroid cultured cells of human pancreatic adenocarcinoma (BxPC3) *in vitro*. Polymeric micelles with their size precisely controlled below 50 nm display great permeability against tumour tissues.[21] Thus, time-dependent internalizations of SOSG@Cy5-PIC/m in both cell culture systems were observed by confocal laser scanning microscopy (CLSM) (Fig. 3a–c). The internalization of the micelle in each cell was evaluated as relative fluorescent units (RFU) per cell or spheroid. The cells cultured in monolayer showed a time-dependent increase in RFU per cell, which became saturated at 6 h incubation (Fig. 3b). Spheroid cultured cells also showed a time-dependent increase of the RFU/spheroid signal. However, the fluorescence intensity in the spheroids kept increasing even after 24 h incubation (Fig. 3c).

The time-dependent penetration of the SOSG@Cy5-PIC/m into the spheroid core of SOSG@Cy5-PIC/m was analysed by taking the fluorescence profile across the spheroids and summarised as histograms (Fig. 3c). These histograms indicate that the SOSG@Cy5-PIC/m penetrated the spheroids time-dependently. At 1 h incubation, the micelles were barely detected in the periphery of the spheroids. Extending the incubation time to 3–6 h increased the micelle-derived fluorescence in cells located at the surface of the spheroids. This also resulted in a gradual decay of the fluorescence profile toward the spheroid core. After 24 h incubation, the micelles were observed throughout the entire spheroid, including the centre of the spheroid. These results suggest that imaging the spheroid culture at 24 h is an optimal time point for detecting $^1O_2$, as the micelles are distributed throughout the entire cluster of cells.

Spheroids more accurately mimic the 3D structure, cell–cell interactions, and microenvironment of tissues *in vivo* compared to monolayer cultures. Therefore, we addressed the proof-of-concept for *in situ* detection of $^1O_2$ by using SOSG@Cy5-PIC/m in BxPC3 spheroids. In this experiment, oxaliplatin, which is a clinically approved drug that can induce $^1O_2$ by mitochondria damage,[12] was used as a trigger for activating the SOSG signal in the micelles. Thus, free SOSG and SOSG@Cy5-PIC/m were first incubated with the spheroid-

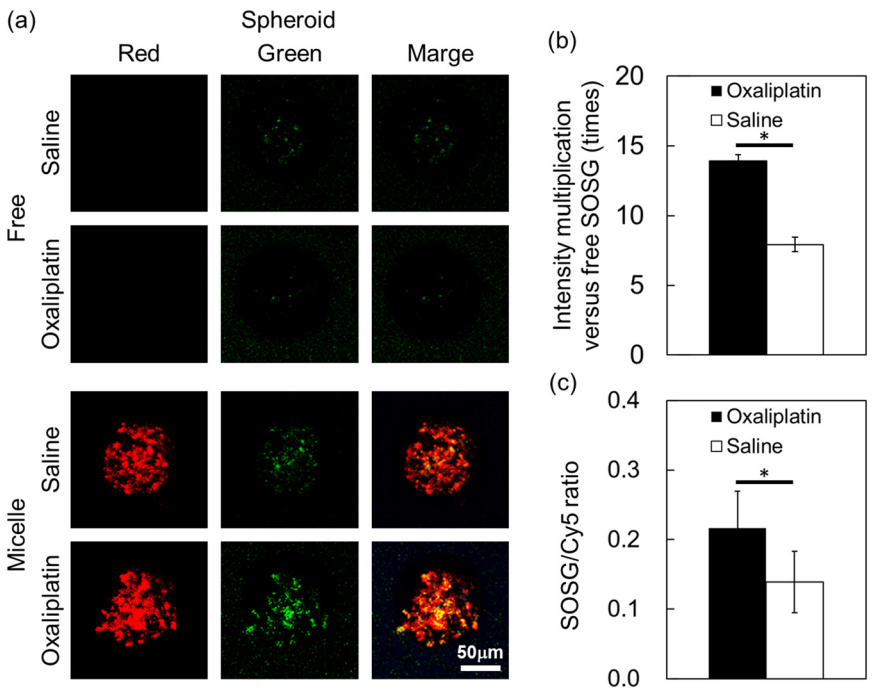

Fig. 4 (a) Fluorescent imaging analysis of SOSG@Cy5-PIC/m against spheroidal cultured BxPC3 cells with oxaliplatin for 24 h co-incubation (red: Cy5 [Ex/Em = 633/661–750 nm], green: SOSG-EP [Ex/Em = 488/499–552 nm], yellow: colocalised micelles and SOSG). Scale bar: 50 μm. (b) Fluorescent intensity of oxaliplatin-stimulated SOSG in the micelles *versus* free SOSG with spheroidal culture. (c) Fluorescent intensity ratio of SOSG/Cy5 in the spheroidal culture. The fluorescence intensity of SOSG/Cy5 per spheroid was calculated. Error bar means standard deviation (n = 4), and all plots were statistically analysed by the Student's t-test (*$p < 0.05$).

cultured BxPC3 cells for 24 h. Then, oxaliplatin was administrated to the cells and incubated for 1, 3, 6 and 24 h to induce $^1O_2$ generation. The distribution of the micelles and the generation of $^1O_2$ inside the cells were imaged by CLSM. The SOSG signal from free SOSG and SOSG@Cy5-PIC/m was not observed in the cells exposed to oxaliplatin for 1 to 6 h (data not shown). However, the $^1O_2$ molecules produced after 24 h incubation with oxaliplatin were detectable by the SOSG in the SOSG@Cy5-PIC/m (Fig. 4a). In contrast, the signal from free SOSG was undetectable. Previous studies have indicated that the access of SOSG into living mammalian cells presents major hurdles[25] and that SOSG is sensitive to extracellular $^1O_2$ molecules, which activates the probes before being internalized by the cells.[27] A comparison of the fluorescence intensity between free SOSG and SOSG@Cy5-PIC/m revealed a 15-fold increase in the SOSG signal intensity (Fig. 4b). The fluorescence intensities of the SOSG in SOSG@Cy5-PIC/m per spheroid were also evaluated by normalizing the SOSG signal with the Cy5 signal (Fig. 4c). Compared to the spheroids treated with saline, the oxaliplatin-treated spheroids showed almost 2-fold higher SOSG/Cy5 ratio ($p < 0.05$). These results support the ability of SOSG@Cy5-PIC/m to detect $^1O_2$ in cellular systems. Given that ROS generation is commonly employed to induce cell death in cancer therapies, SOSG@Cy5-PIC/m offers a valuable tool for monitoring the therapeutic efficacy of such treatments. Additionally, the system's capability to encapsulate ROS-generating drugs, such as oxaliplatin used in this study, within its core enables a theranostic approach that can simultaneously treat and track therapeutic effects with a single carrier. With further improvements and tuning, SOSG@Cy5-PIC/m holds the potential of introducing a new paradigm in cancer theranostics, enabling the concurrent generation and detection of ROS.

Conclusions

We successfully developed SOSG/Cy5-labeled PIC/m as a probe for the detection of $^1O_2$ in biological environments. The SOSG@Cy5-PIC/m probes were internalised by BxPC3 pancreatic cancer cells in a time-dependent manner and were able to penetrate into the core of spheroidal cultures of BxPC3 cells. Thus, using these probes, we successfully detected the *in situ* $^1O_2$ generated by oxaliplatin in the spheroids. This method shows promise for the local analysis and quantification of $^1O_2$ in biological systems. The SOSG/Cy5-labeled PIC/m could be applied in a wide variety of treatments based on the oxidative responses, leading to an improved understanding of biological mechanisms, diagnostic tools, and therapeutic strategies.

Data availability

The authors confirm that the data supporting the findings of this study are available within the article. Raw data that support the findings of this study are available from the corresponding author, upon reasonable request.

Conflicts of interest

There are no conflicts to declare.

Acknowledgements

This work was supported by Grants-in-Aid for Scientific Research A (23H00546; H. C.), Grants-in-Aid for Exploratory Research (22K19541; H. C.), and the Fund for the Promotion of Joint International Research (Fostering Joint International Research (B), 21KK0197; H. C.), from the Japan Society for the Promotion of Science (JSPS). This work was also partially supported by the AMED Seeds A grant (23ym0126805j0002; H. C.).

References

1 T. Finkel and N. J. Holbrook, *Nature*, 2000, **408**, 239–247.
2 B. Halliwell and J. M. Gutteridge, *Free radicals in biology and medicine*, Oxford University Press, USA, 2015.
3 M. Schieber and N. S. Chandel, *Curr. Biol.*, 2014, **24**, R453–R462.
4 R. Scherz-Shouval and Z. Elazar, *Trends Biochem. Sci.*, 2011, **36**, 30–38.
5 G. Lenaz, *IUBMB Life*, 2001, **52**, 159–164.
6 G. Kojda and D. Harrison, *Cardiovasc. Res.*, 1999, **43**, 652–671.
7 G.-Y. Liou and P. Storz, *Free Radical Res.*, 2010, **44**, 479–496.
8 H. Yang, R. M. Villani, H. Wang, M. J. Simpson, M. S. Roberts, M. Tang and X. Liang, *J. Exp. Clin. Cancer Res.*, 2018, **37**, 266.
9 R. L. Berkow, D. Wang, J. W. Larrick, R. W. Dodson and T. H. Howard, *J. Immunol.*, 1987, **139**, 3783.
10 A. Ibrahim, S. Hirschfeld, M. H. Cohen, D. J. Griebel, G. A. Williams and R. Pazdur, *Oncologist*, 2004, **9**, 8–12.
11 H. Zheng, W. H. Xiao and G. J. Bennett, *Exp. Neurol.*, 2011, **232**, 154–161.
12 V. Santoro, R. Jia, H. Thompson, A. Nijhuis, R. Jeffery, K. Kiakos, A. R. Silver, J. A. Hartley and D. J. Hochhauser, *Natl. Cancer Inst.*, 2016, **108**, djv394.
13 N. M. Hasty and D. R. Kearns, *J. Am. Chem. Soc.*, 1973, **95**, 3380–3381.
14 M. Bobrowski, A. Liwo, S. Ołdziej, D. Jeziorek and T. Ossowski, *J. Am. Chem. Soc.*, 2000, **122**, 8112–8119.
15 A. Baker and J. R. Kanofsky, *Arch. Biochem. Biophys.*, 1991, **286**, 70–75.
16 J. Moan and E. Wold, *Nature*, 1979, **279**, 450–451.
17 A. Telfer, S. M. Bishop, D. Phillips and J. Barber, *J. Biol. Chem.*, 1994, **269**, 13244–13253.
18 C. Flors, M. J. Fryer, J. Waring, B. Reeder, U. Bechtold, P. M. Mullineaux, S. Nonell, M. T. Wilson and N. R. Baker, *J. Exp. Bot.*, 2006, **57**, 1725–1734.
19 A. Krasnovsky Jr, *Membr. Cell Biol.*, 1998, **12**, 665–690.
20 J. Baier, T. Fuß, C. Pöllmann, C. Wiesmann, K. Pindl, R. Engl, D. Baumer, M. Maier, M. Landthaler and W. Bäumler, *J. Photochem. Photobiol. B*, 2007, **87**, 163–173.

21 H. Cabral, K. Miyata, K. Osada and K. Kataoka, *Chem. Rev.*, 2018, **118**, 6844–6892.
22 M. E. Davis, Z. Chen and D. M. Shin, *Nat. Rev. Drug Discov.*, 2008, **7**, 771–782.
23 A. Wibowo, K. Osada, H. Matsuda, Y. Anraku, H. Hirose, A. Kishimura and K. Kataoka, *Macromolecules*, 2014, **47**, 3086–3092.
24 Y. Anraku, H. Kuwahara, Y. Fukusato, A. Mizoguchi, T. Ishii, K. Nitta, Y. Matsumoto, K. Toh, K. Miyata, S. Uchida, K. Nishina, K. Osada, K. Itaka, N. Nishiyama, H. Mizusawa, T. Yamasoba, T. Yokota and K. Kataoka, *Nat. Commun.*, 2017, **8**, 1001.
25 A. Gollmer, J. Arnbjerg, F. H. Blaikie, B. W. Pedersen, T. Breitenbach, K. Daasbjerg, M. Glasius and P. R. Ogilby, *Photochem. Photobiol.*, 2011, **87**, 671–679.
26 H. Lin, Y. Shen, D. Chen, L. Lin, B. C. Wilson, B. Li and S. Xie, *J. Fluoresc.*, 2013, **23**, 41–47.
27 Y. Shen, H. Y. Lin, Z. F. Huang, D. F. Chen, B. H. Li and S. Xie, *Laser Phys. Lett.*, 2011, **8**, 232–238.